High-Resolution Simulation of Multidimensional Crystal Growth

David L. Ma, Danesh K. Tafti,[†] and Richard D. Braatz*

Department of Chemical Engineering, University of Illinois, Urbana, Illinois 61801

Many of the crystals in the pharmaceuticals, photographic, and other industries are multidimensional; that is, their growth is associated with the change of multiple internal coordinates. The main governing equation for such systems is a highly nonlinear multidimensional population balance equation that must be solved for a wide range of length scales. For population balance equations, it is well-known that the standard first-order schemes give diffusive solutions while the commonly used second-order schemes give spurious oscillations. This paper presents a high-resolution simulation algorithm that provides short computation times and high accuracy. The high-resolution algorithm is compared to the upwind difference and Lax−Wendroff methods through simulations of potassium dihydrogen phosphate (KDP, KH_2PO_4) crystal nucleation and growth. No spurious oscillations or numerical diffusion occurred, in contrast to the upwind method and Lax−Wendroff methods. The numerical stability of the algorithm is assessed using the Courant−Friedrichs−Lewy condition.

1. Introduction

Many of the crystals in the pharmaceuticals, photographic, and other industries are multidimensional; that is, their growth is associated with the change of multiple internal coordinates.[1] Such internal coordinates can include volume, mass, length, width, composition, or the number of crystals in an agglomerate. The main roadblock to gaining further understanding of multidimensional crystal growth, as well as the development of optimal control strategies for these processes, is the lack of efficient simulation schemes for multidimensional population balance equations. Although there is a rapidly growing experimental literature on multidimensional crystal growth from solution[2−7] and a large amount of industrial interest, simulation studies of multidimensional crystal growth are nearly nonexistent.

Most simulation studies on crystal growth have been directed toward the solution of the population balance equation for one-dimensional (1D) crystal growth:[8−12]

$$\frac{\partial f}{\partial t} + \frac{\partial \{ G[c(t), T(t), r]f \}}{\partial r} = h(r, t) \tag{1}$$

where $f(r,t)$ is the crystal size distribution, t is time, r is the internal spatial coordinate (e.g., crystal size), c is the solute concentration, T is the temperature, G is the growth function, and h is the crystal creation/depletion function. This equation is augmented with associated algebraic and/or integrodifferential equations to describe the energy balance, aggregation, breakage, growth, and nucleation phenomena. Simulating these equations is challenging because the crystal size distribution can be extremely sharp in practice and can span many orders of magnitude in crystal length scale (0.01 nm to 200 μm) and time scale (20 μs to 200 min).

Numerical schemes developed for the simulation of 1D crystal growth cannot be directly applied to the simulation of multidimensional crystal growth. It is well-known that the standard first-order schemes give diffusive solutions while the commonly used second-order schemes give spurious oscillations.[13] This paper presents a simulation algorithm that has second-order accuracy but does not produce spurious oscillations, based on *high-resolution methods* that have been developed for solving hyperbolic partial differential equations.[14−18] The algorithm obtains second-order accuracy by using a first-order scheme supplemented with limited antidiffusion terms. The high-resolution algorithm is compared to the popular upwind difference and Lax−Wendroff methods through simulations of potassium dihydrogen phosphate (KDP, KH_2PO_4) crystal nucleation and growth.

2. High-Resolution Algorithm

For a well-mixed crystallizer in which the crystals have two characteristic length scales, the process is described by the population balance equation:[1,19]

$$\frac{\partial f}{\partial t} + \sum_{j=1}^{2} \frac{\partial \{ G_j[c(t), T(t)]f \}}{\partial r_j} = h(t) \tag{2}$$

where f is the crystal size distribution, r_j refers to each characteristic length scale, G_j refers to the growth rate for the jth length scale, and c is the solute concentration. The function h is the net rate of introduction of new crystals into the system, whether via feed or exit streams or by processes of nucleation, breakage, attrition, and agglomeration occurring in the crystallizer.

The population balance equation (2) is a multidimensional conservation equation. Standard first- and second-order approximation methods have difficulties accurately simulating this equation when there are sharp gradients in its solution. In the literature, the first-order approximation methods are often used with special consideration to selecting the mesh size in order to reduce numerical diffusion. Standard higher order approximation methods give spurious oscillations, which usually result in a crystal size distribution with negative values.[13]

* To whom correspondence should be addressed. Fax: 217-333-5052. Phone: 217-333-5073. E-mail: braatz@uiuc.edu.
† Present address: Mechanical Engineering Department, Virginia Polytechnic Institute and State University, 114 Randolph Hall, Blacksburg, VA 24061.

High-resolution methods have been developed, primarily by the computational physics community,[14−18] to address the numerical problems associated with standard algorithms for solving hyperbolic equations. High-resolution algorithms can handle large gradients while retaining second-order accuracy for all or almost all of the solution space. However, most high-resolution methods have been developed for 1D conservation equations. While some of the direct extensions of 1D high-resolution methods do not produce higher than first-order accuracy for the 2D problem,[20] second-order accurate 2D high-resolution methods can be developed provided that some care is placed in the formulation.[15]

To solve (2), a splitting method is used to decompose (2) into a pair of 1D equations. A high-resolution method is used to solve each of the two 1D equations. While most high-resolution methods have been developed for equations in which the right-hand side of (2) is zero, the crystal creation rate $h(t)$ in (2) can be quite large and numerically behaves like a source term (although this term is a function of the crystal size distribution). This equation can be solved by first solving the homogeneous equation

$$\frac{\partial f}{\partial t} + \sum_{j=1}^{2} \frac{\partial \{G_j[c(t), T(t)]f\}}{\partial r_j} = 0 \tag{3}$$

over time step k and then adding the new crystals to the appropriate cell(s) over the same time increment.[16] The following analysis will focus on how to solve (3) with second-order accuracy.

Some definitions will aid in the following discussion. For the 1D conservation equation, the grid points are defined as the points $(t_m, r_n) = (mk, nh)$ for positive integers m and n, where h is the mesh size and k is the time step. To simplify the presentation, assume that the ratio of k and h is constant. Let f_n^m be the population density function f defined on the grid point (t_m, r_n).

At time instant t_{m-1}, (3) is

$$\frac{\partial f}{\partial t} + g_1^{m-1} \frac{\partial f}{\partial r_1} + g_2^{m-1} \frac{\partial f}{\partial r_2} = 0 \tag{4}$$

with initial crystal size distribution

$$f = f^{m-1}(r_1, r_2) \tag{5}$$

The analytical solution to this partial differential equation (PDE) at t_m is

$$f = f^{m-1}(r_1 - g_1^{m-1}(t_m - t_{m-1}), r_2 - g_2^{m-1}(t_m - t_{m-1})) \tag{6}$$

Now recognize that the same PDE can be solved in two steps. First, the 1D PDE

$$\frac{\partial \hat{f}}{\partial t} + g_1^{m-1} \frac{\partial \hat{f}}{\partial r_1} = 0 \tag{7}$$

$$\hat{f} = f^{m-1}(r_1, r_2) \qquad \text{at } t = t_{m-1} \tag{8}$$

is solved. The solution to this PDE is $\hat{f}^m(r_1, r_2) = f^{m-1}(r_1 - g_1^{m-1}(t_m - t_{m-1}), r_2)$. Now use $\hat{f}$ as the initial condition to solve the second PDE

$$\frac{\partial \tilde{f}}{\partial t} + g_2^{m-1} \frac{\partial \tilde{f}}{\partial r_2} = 0 \tag{9}$$

$$\tilde{f} = \hat{f}^m(r_1, r_2) \qquad \text{at } t = t_{m-1} \tag{10}$$

The solution to the second PDE at t_m is identical to the solution (6):

$$\tilde{f}(r_1, r_2) = \hat{f}^m(r_1, r_2 - g_2^{m-1}(t_m - t_{m-1})) = f^{m-1}(r_1 - g_1^{m-1}(t_m - t_{m-1}), r_2 - g_2^{m-1}(t_m - t_{m-1})) \tag{11}$$

The above derivation illustrates that the 2D PDE (3) can be solved by first splitting it to a pair of 1D PDEs along r_1 and r_2 and solving the two PDEs separately at each time step. Then the two solutions can be combined to form the solution to the original PDE.

This analytical development motivates the numerical algorithm discussed next. After splitting and at each time instant, a high-resolution method is applied to solve the 1D equation

$$\frac{\partial f}{\partial t} + g \frac{\partial f}{\partial r} = 0 \tag{12}$$

with the initial condition $f(r) = \tilde{f}(r)$. The high-resolution method used here is a hybrid of the upwind method and Lax−Wendroff method.[15] The upwind method is a first-order finite difference method that replaces $\partial f/\partial t$ by a forward-in-time approximation and $\partial f/\partial r$ by a backward finite difference:

$$f_n^{m+1} = f_n^m - \frac{k}{h}g(f_n^m - f_{n-1}^m) \tag{13}$$

The main drawback of this method is that it exhibits severe numerical diffusion. The Lax−Wendroff method gives second-order accuracy and eliminates numerical diffusion:

$$f_n^{m+1} = f_n^m - \frac{kg}{2h}(f_{n+1}^m - f_{n-1}^m) + \frac{k^2 g^2}{2h^2}(f_{n+1}^m - 2f_n^m + f_{n-1}^m) \tag{14}$$

A drawback of this method is that it adds spurious oscillations. The population density can have negative values when the local gradients are large. Rewriting the Lax−Wendroff method provides insight into the cause of oscillation:

$$f_n^{m+1} = f_n^m - \frac{kg}{h}(f_n^m - f_{n-1}^m) - \frac{kg}{2h}\left(1 - \frac{kg}{h}\right)[(f_{n+1}^m - f_n^m) - (f_n^m - f_{n-1}^m)] \tag{15}$$

Equation 15 shows that the Lax−Wendroff method essentially consists of first-order upwind method, supplemented with an antidiffusion term

$$\frac{kg}{2h}\left(1 - \frac{kg}{h}\right)[(f_{n+1}^m - f_n^m) - (f_n^m - f_{n-1}^m)] \tag{16}$$

This antidiffusion term prevents numerical diffusion, but the magnitude of this term is too large near discontinuities, causing undesirable oscillations. To remedy this, the high-resolution method restricts the magnitude of this antidiffusion term:

$$f_n^{m+1} = f_n^m - \frac{kg}{h}(f_n^m - f_{n-1}^m) - \frac{kg}{2h}\left(1 - \frac{kg}{h}\right)[(f_{n+1}^m - f_n^m)\phi_n - (f_n^m - f_{n-1}^m)\phi_{n-1}] \tag{17}$$

The term ϕ_n is called a limiter, whose value depends on the local gradients. Define θ_n as the ratio of the local gradients

$$\theta_n = \frac{f_n{}^m - f_{n-1}{}^m}{f_{n+1}{}^m - f_n{}^m} \qquad (18)$$

and let ϕ_n be a function of the local gradients so that $\phi_n = \phi(\theta_n)$. It is desired for the limiter function ϕ to be selected so that it provides second-order accuracy while not producing any spurious oscillation. It can be shown[15,18] that these requirements are satisfied if ϕ is Lipschitz continuous at $\theta = 1$, $\phi(1) = 1$,

$$0 \leq \frac{\phi(\theta_n)}{\theta_n} \leq 2 \qquad (19)$$

and

$$0 \leq \phi(\theta_n) \leq 2 \qquad (20)$$

Many choices for the limiter function ϕ are available. Comparisons of various limiter functions are available.[18,21] We have found a good performance with[22]

$$\phi(\theta_n) = \frac{|\theta_n| + \theta_n}{1 + |\theta_n|} \qquad (21)$$

3. Simulation Examples

3.1. Solving the 1D Advection Equation. To illustrate clearly the advantages of the high-resolution algorithm, it is compared with the upwind and Lax–Wendroff methods applied to the PDE (12) (see Figure 1). In this case analytical solution to PDE (12) is simply a copy of the initial function shifted to the right by gt_{final}. The wave speed g in the simulation is set to 0.2 μm/s, and the mesh size and time step are set to 1 μm and 1 s, respectively. The simulation results show that the upwind method gives a smeared solution while the Lax–Wendroff method gives an oscillatory solution. The high-resolution method nearly preserves the shape of the initial function.

The diffusive behavior of the upwind algorithm can be understood by modeling its difference equation by a new PDE for which the difference equation provides a better approximation. For the upwind method, the new PDE can be chosen as the advection–diffusion equation[15]

$$f_t + gf_r = \frac{1}{2}hg\left(1 - \frac{k}{H}g\right)f_{rr} \qquad (22)$$

The upwind algorithm is second-order accurate for solving this PDE. The PDE predicts that, when applying the upwind method to the simulation of crystallization, the crystal size distribution will propagate with the speed g while being dissipated with diffusion coefficient $\frac{1}{2}hg(1 - khg)$ as time evolves.

The dispersive behavior of the Lax–Wendroff method can be understood by noting that its difference equation provides a third-order accurate solution to the dispersive PDE

$$f_t + gf_r = \frac{h^2g}{6}\left(\frac{k^2}{h^2}g^2 - 1\right)f_{rrr} \qquad (23)$$
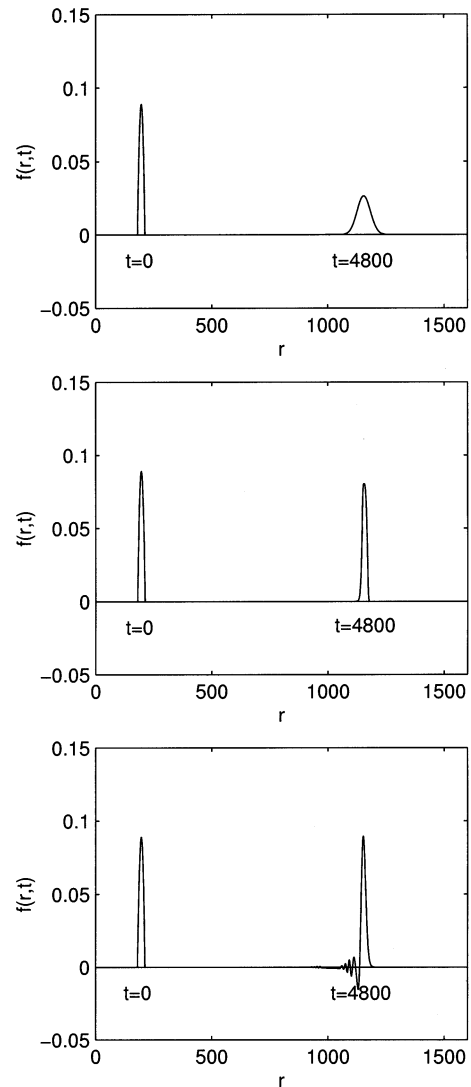

Figure 1. Numerical solution to (12) using the upwind, high-resolution, and Lax-Wendroff methods.

Fourier analysis shows that the Fourier components with different wavenumber ξ propagate at different speeds (see refs 15 and 23 for a detailed analysis). As time evolves, these components disperse, leading to an oscillatory solution.

3.2. Simulation of 2D Crystal Growth. Now the algorithms are applied to the formation of crystals with two characteristic length scales (2). KDP is selected because both its nucleation kinetics and growth kinetics along each crystal growth axis have been identified from experimental data. The shape of KDP crystals is tetragonal prism in combination with tetragonal bipyramid, and the angle between the prism sides and the pyramid faces is 45°.[24,25] The two internal dimensions r_1 and r_2 are the width and length of the KDP crystal, respectively (see Figure 2). Accordingly, the volume of a single crystal is

$$V_c = \frac{1}{3}r_1{}^3 + (r_2 - r_1)r_1{}^2 \qquad (24)$$

The numerical algorithms are applicable to any of the many crystal growth and nucleation mechanisms and their associated rate expressions described in the literature.[26-30] For the KDP–water system, many researchers have experimentally observed that the growth
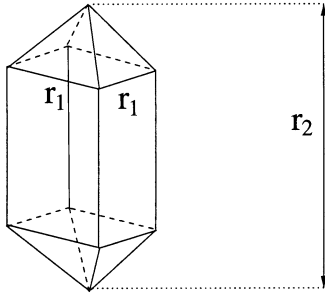
Figure 2. Shape of KDP crystals.

Table 1. Kinetic Parameters Determined from Laboratory Data[32]

parameter	value	units
g_1	1.48	dimensionless
k_{g_1}	12.21	μm/s
g_2	1.74	dimensionless
k_{g_2}	100.75	μm/s
b	2.04	dimensionless
k_b	7.49×10^{-8}	particles/μm$^3\cdot$s

Table 2. Parameters Used in Simulation

variable	description	value	units
k	time step	5	s
h	mesh size	1	μm
V	volume	2	L
t	batch time	2	h
T_{init}	initial temperature	33	°C
T_{final}	final temperature	23	°C
t_{sim}	simulation time	10	min

kinetics for each axis can be represented as a power law function of the supersaturation:[25,31,32]

$$G_1 = k_{g_1}\left(\frac{c - c_{sat}}{c_{sat}}\right)^{g_1} = k_{g_1}S^{g_1} \qquad (25)$$

$$G_2 = k_{g_2}\left(\frac{c - c_{sat}}{c_{sat}}\right)^{g_2} = k_{g_2}S^{g_2} \qquad (26)$$

where c is the solute concentration, c_{sat} is the saturated solute concentration, S is the relative supersaturation, and g_1, g_2, k_{g_1}, and k_{g_2} are kinetic parameters. The particular kinetic parameters used in this study were identified by applying nonlinear parameter estimation and model-based experimental design to batch crystallization data (see Table 1). The saturated solute concentration c_{sat} for KDP is[33]

$$c_{sat} = 9.3027 \times 10^{-5}T^2 - 9.7629 \times 10^{-5}T + 0.2087 \qquad (27)$$

where T is the temperature in degrees Celsius and the units for c_{sat} are g/g of water.

Before crystallization starts, seed crystals are added to the solution to avoid spontaneous nucleation from solution. The initial seed crystal size distribution is shown in Figure 3. Secondary nucleation is the dominant mechanism for producing new crystals in most seeded batch crystallizers. This type of nucleation kinetics is usually characterized as being proportional to either the area or volume of crystals in the crystallizer. In this paper, the latter is assumed:

$$h(t) = k_b\left(\frac{c - c_{sat}}{c}\right)^b \delta(r_1)\,\delta(r_2) \int_0^\infty \int_0^\infty f(r_1,r_2,t) \\ V_c(r_1,r_2)\,dr_1\,dr_2 \qquad (28)$$

where δ is the Dirac delta function. The nucleation kinetic parameters are reported in Table 1.

A solute mass balance completes the model for a batch crystallizer. With the assumption that nucleated crystals have negligible size (a good assumption in practice), the amount of solute leaving the solution must be accounted by crystal growth. For KDP this equation is

$$\frac{dC}{dt} = -\rho_c\int_0^\infty \int_0^\infty f(r_1,r_2,t)\,(2\,G_1(r_1r_2 - r_1^2) + \\ G_2r_1^2)\,dr_1\,dr_2 \qquad (29)$$

where ρ_c is the crystal density ($\rho_c = 2.338 \times 10^{-12}$ g/μm^3 in the simulation).

The following discussion of the algorithms uses cross-moments:

$$\mu_{ij} = \int_0^\infty \int_0^\infty f(r_1,r_2,t)\,r_1^i r_2^j\,dr_1\,dr_2 \qquad (30)$$

The low-order moments have physical meaning; for example, μ_{00} is the total number of crystals in the system per gram of solvent, and μ_{10}/μ_{00} is the average width of the crystals.

While the algorithms have been applied to a wide range of batch and continuous operating conditions,[34] only a subset of the results are provided here because the qualitative comparisons are similar in the other cases. Here the crystallizer is cooled linearly, and the temperature is assumed to be uniform throughout the crystallizer. These conditions are selected because they are the easiest for use in comparing the accuracy of the numerical algorithms. Readers interested in much more complex and interesting dynamics and changes in the crystal size distribution are referred to the first author's thesis.[34]

Parameters used in the simulation are summarized in Table 2. The initial and final crystal size distributions obtained from the three simulation algorithms are shown in Figure 3. All of the seed crystals had an aspect ratio nearly equal to 1. Each final crystal size distribution shows two distributions, one associated with crystals that grew from seeds and the other associated with crystals grown from nuclei. For the high-resolution method, the average length of crystals grown from seeds is around 800 μm and the average width is around 350 μm, indicating that the crystals are becoming elongated. The size of the nuclei is small, and hence nucleated crystals appear at the origin. As time evolves, the nucleated crystals grow larger in such a way that their aspect ratios are nearly constant. No oscillations or severe numerical diffusion are observed.

In contrast, the upwind method exhibits severe numerical diffusion. The distribution of the crystal grown from seeds becomes very flat as the final time is reached. The Lax−Wendroff method does not exhibit numerical diffusion, but it gives an extremely oscillatory solution. The final crystal size distribution has negative values which are not physically possible.

The crystallization system used in this paper can be simulated by using the method of moments,[19] which is used to determine the accuracy of the crystal size
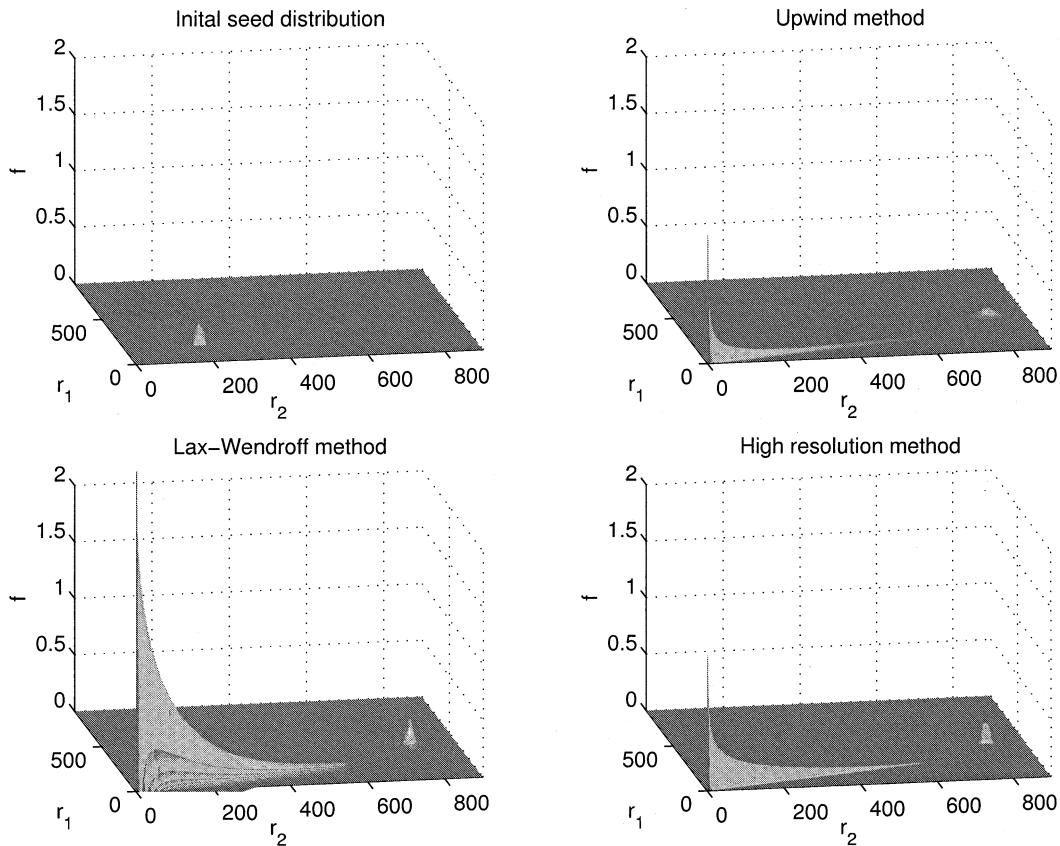
Figure 3. Initial seed distribution and final crystal size distribution generated by the upwind, Lax−Wendroff, and high-resolution methods.
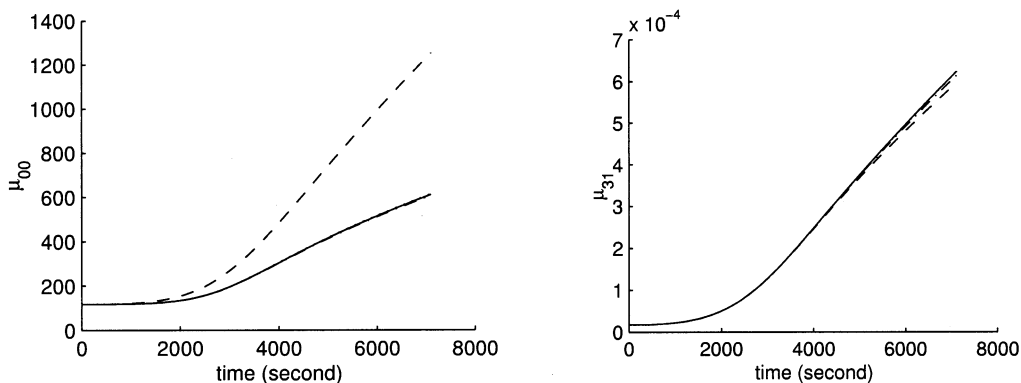

Figure 4. Cross moments μ_{00} and μ_{31} computed using the method of moments (···) and the upwind (− · −), Lax−Wendroff (− − −), and high-resolution methods (−).

distributions computed from the simulation algorithms. The obtained moments are compared with corresponding moments computed directly from the crystal size distribution which is obtained from the high-resolution, upwind, and Lax−Wendroff methods. The moment μ_{00} computed from the Lax−Wendroff method is much larger than its true value, whereas the high-resolution and upwind methods are accurate (see Figure 4). The overestimation by the Lax−Wendroff method is due to the large oscillations produced by the Lax−Wendroff method. The upwind and Lax−Wendroff methods are much less accurate than the high-resolution algorithm for all moments. For example, for μ_{31} the high-resolution method has relative errors of less than 0.001 (the lines for the method of moments and the high-resolution algorithms are indistinguishable), whereas the errors in the upwind and Lax−Wendroff methods are clear in Figure 4.

A necessary condition for any numerical algorithm to be numerically stable is the Courant−Friedrichs−Lewy (CFL) condition:[35]

$$|gk/h| \leq 1 \qquad (31)$$

This stability condition requires that the domain of dependence of the finite difference method should include the domain of dependence of the PDE. In the case of the high-resolution method, this requires that the numerical wave speed h/k be faster than the wave speed in the PDE. For the two-dimensional crystallization of KDP, the magnitude of the crystal growth rate is less than 0.1 μm/s during the entire simulation run. As a result, the time step k can be chosen as relatively large to reduce the simulation time. To satisfy the CFL condition, the ratio k/h can be selected to be 5, which provides numerical stability and keeps the final errors small. The speed of the simulation can be further

increased by recognizing that *f* has the nonzero values only in the regions where nucleation has occurred or the seed crystals reside. The high-resolution method is only needed in these two regions. The overall computation effort is then dramatically reduced. An easy-to-implement method to define regions where *f* may not be zero at time t_n can be done as follows. Assume that initially the two regions can be approximated by two rectangular sets:

$$\mathscr{R}_{\text{seed}} = \{(r_1, r_2): \ p_1 \leq r_1 \leq p_2 \text{ and } q_1 \leq r_2 \leq q_2\} \quad (32)$$

and

$$\mathscr{R}_{\text{nucleation}} = \{(r_1, r_2): \ 0 \leq r_1 \leq p_3 \text{ and } 0 \leq r_2 \leq q_3\} \quad (33)$$

The set $\mathscr{R}_{\text{nucleation}}$ grows bigger as the crystals grown from nuclei become bigger, while the size of the set $\mathscr{R}_{\text{seed}}$ is fixed. The set $\mathscr{R}_{\text{seed}}$ shifts to the region of larger values of r_1 and r_2 as time evolves. At time t_n, the two sets can be approximated as

$$\mathscr{R}_{\text{seed}} = \{(r_1, r_2): \ p_1 + \int_0^{t_n} G_1(t) \, dt \leq r_1 \leq p_2 + \int_0^{t_n} G_1(t) \, dt \text{ and } q_1 + \int_0^{t_n} G_2(t) \, dt \leq r_2 \leq q_2 + \int_0^{t_n} G_2(t) \, dt\} \quad (34)$$

and

$$\mathscr{R}_{\text{nucleation}} = \{(r_1, r_2): \ 0 \leq r_1 \leq p_3 + \int_0^{t_n} G_1(t) \, dt \text{ and } 0 \leq r_2 \leq q_3 + \int_0^{t_n} G_2(t) \, dt\} \quad (35)$$

Using the above techniques, the overall simulation time was reduced to 2 min on a HP Kayak Visualize Workstation with dual Pentium III Xeon 550 MHz processors and 1 GB of memory.

4. Conclusion

A high-resolution method was developed that simulates the dynamics of a multidimensional crystallization process. The high-resolution method provides short computation times and high accuracy. No spurious oscillations or numerical diffusion occurred, in contrast to the upwind method and Lax−Wendroff methods. With reduction of the computation domain, the final simulation time for a 2D crystallization process was reduced to 2 min on a dated personal computer.

Acknowledgment

Literature Cited

(1) Braatz, R. D.; Hasebe, S. Particle size and shape control in crystallization processes. In *Chemical Process Control VI*; Rawlings, J. B., Ogunnaike, B. A., Eds.; AIChE Press: New York, 2001; in press.

(2) Brown, P. M.; Myerson, A. S. The growth, dissolution and aging of terephthalic acid crystals. *AIChE J.* **1989**, *35*, 1749.

(3) Gabas, N.; Lauerie, C. Dispersion on growth rates of D-xylose crystals in aqueous solutions−influence of the presence of ethanol as a cosolvent and of D-mannose as a cosolute. *Chem. Eng. Sci.* **1991**, *46*, 1411.

(4) Myerson, A. S.; Saska, M. Formation of solvent inclusions in terephthalic acid crystals. *AIChE J.* **1984**, *30*, 865.

(5) Saska, M.; Myerson, A. S. Crystal aging and crystal habit of terephthalic acid. *AIChE J.* **1987**, *33*, 848.

(6) Togkalidou, T.; Braatz, R. D. Inferential modeling in pharmaceutical crystallization. In *Proceedings of the American Control Conference*; IEEE Press: Piscataway, NJ, 1999; p 2548.

(7) Togkalidou, T.; Johnson, B. K.; Braatz, R. D.; Davidson, O.; Andrews, A. Experimental design and inferential modeling in pharmaceutical crystallization. *AIChE J.* **2001**, *47*, 160.

(8) Hill, P. J.; Ng, K. M. New distribution procedure for the breakage solution. *AIChE J.* **1995**, *41*, 1204.

(9) Kumar, S.; Ramkrishna, D. On the solution of population balance equations by discretization−I. a fixed pivot technique. *Chem. Eng. Sci.* **1996**, *51*, 1311.

(10) Litster, J. D.; Smit, D. J.; Hounslow, M. J. Adjustable discretized population balance for growth and aggregation. *AIChE J.* **1995**, *41*, 591.

(11) Marchal, P.; David, R.; Klein, J. P.; Villermaux, J. Crystallization and precipitation engineering. I: An efficient method for solving population balance in crystallization with agglomeration. *Chem. Eng. Sci.* **1988**, *43*, 59.

(12) Muhr, H.; David, R.; Villermaux, J.; Jezequel, P. H. Crystallization and precipitation engineering−VI. Solving population balance in the case of the precipitation of silver bromide crystals with high primary nucleation rates by using the first-order upwind differentiation. *Chem. Eng. Sci.* **1996**, *51*, 309.

(13) Sotowa, K.; Naito, K.; Kano, M.; Hasebe, S.; Hashimoto, I. Application of the method of characteristics to crystallizer simulation and comparison with finite difference for controller performance evaluation. *J. Process Control* **2000**, *10*, 203.

(14) Harten, A. High-resolution schemes for hyperbolic conservation laws. *J. Comput. Phys.* **1983**, *49*, 357.

(15) LeVeque, R. J. *Numerical Methods for Conservation Laws*; Birkhäuser Verlag: Basel, Germany, 1992.

(16) LeVeque, R. J. Wave propagation algorithms for multidimensinal hyperbolic systems. *J. Comput. Phys.* **1997**, *131*, 327.

(17) Osher, S.; Chakravarthy, S. High-resolution schemes and the entropy condition. *SIAM J. Numer. Anal.* **1984**, *131*, 955.

(18) Sweby, P. K. High-resolution schemes using flux limiters for hyperbolic conservation laws. *SIAM J. Numer. Anal.* **1984**, *21*, 995.

(19) Hulburt, H. M.; Katz, S. Some problems in particle technology. *Chem. Eng. Sci.* **1964**, *19*, 555.

(20) Goodman, J. B.; LeVeque, R. J. On the accuracy of stable schemes for 2D scalar conservation laws. *Math. Comput.* **1985**, *45*, 15.

(21) Zalesak, S. T. A preliminary comparison of modern shock-capturing schemes: linear advection. In *Advances in Computer Methods for Partial Differential Equations*; Vichnevetsky, R., Stepleman, R. S., Eds.; IMACS: Lehigh University, Bethlehem, PA, 1987; Vol. VI.

(22) van Leer, B. Towards the ultimate conservative difference scheme II. Monotonicity and conservation combined in a second-order scheme. *J. Comput. Phys.* **1974**, *14*, 361.

(23) Whitham, G. *Linear and Nonlinear Waves*; Wiley-Interscience: New York, 1974.

(24) Ma, D. L.; Braatz, R. D. Worst-case analysis of finite-time control policies. *IEEE Trans. Control Syst. Technol.* **2001**, *9*, 766.

(25) Mullin, J. W.; Amatavivadhana, A. Growth kinetics of ammonium- and potassium-dihydrogen phosphate crystals. *J. Appl. Chem.* **1967**, *17*, 151.

(26) Burton, W. K.; Cabrera, D. A.; Franck, F. C. The growth of the crystals and the equilibrium structure of their surfaces. *Philos. Trans. R. Soc. London* **1951**, *A243*, 229.

(27) Garside, J. The concept of effectiveness factors in crystal growth. *Chem. Eng. Sci.* **1971**, *26*, 1425.

(28) Hillig, W. B. A derivation of classical two-dimensional nucleation kinetics and the associated crystal growth laws. *Acta Metall.* **1966**, *14*, 1868.

(29) Randolph, A.; Larson, M. A. *Theory of Particulate Processes*, 2nd ed.; Academic Press: San Diego, 1988.

(30) Mersmann, A. Fundamentals of crystallization. In *Crystallization Technology Handbook*; Mersmann, A., Ed.; Marcel Dekker: New York, 1995.

(31) Mullin, J. W.; Amatavivadhana, A.; Chakraborty, M. Crystal habit modification studies with ammonium and potassium dihydrogen phosphate. *J. Appl. Chem.* **1970**, *20*, 153.

(32) Gunawan, R.; Ma, D. L.; Fujiwara, M.; Braatz, R. D. Identification of kinetic parameters in a multidimensional crystallization process. *Int. J. Mod. Phys. B* **2001**, in press (special issue on crystallization and interfacial processes).

(33) Togkalidou, T.; Fujiwara, M.; Patel, S.; Braatz, R. D. Solute concentration prediction using chemometrics and ATR-FTIR spectroscopy. *J. Cryst. Growth* **2001**, *231*, 534.

(34) Ma, D. L. Simulation and Optimization of Industrial Crystallization Processes. Ph.D. Thesis, University of Illinois, Urbana, IL, 2002.

(35) Courant, R.; Friedrichs, K. O.; Lewy, H. Uber die partiellen differenzengleichungen der mathematisches physik. *Math. Ann.* **1928**, *100*, 32.